Supplementary Information

Design of Rhenium–Decorated Mesoporous Nickel Phyllosilicate–Derived Ni–Re/MCM-41 Catalyst for Efficient Hydrogenation of Levulinic Acid to γ-Valerolactone

Yupawan Maneewong[a+], Pratikkumar Lakhani[a+], Sakhon Ratchahat[a], Chularat Sakdaronnarong[a], Wanwisa Limphirat[b,c], Bunyarat Rungtaweevoranit[d], Suttichai Assabumrungrat[e,f], Kanyanat Khosukwiwat[g], Kittisak Choojun[g], Tawan Sooknoi[g], Keiichi Tomishige[h], and Atthapon Srifa[a,*]

[a] Department of Chemical Engineering, Faculty of Engineering, Mahidol University, Nakhon Pathom 73170, Thailand
[b] Synchrotron Light Research Institute, Nakhon Ratchasima, 30000, Thailand
[c] Department of Chemical Engineering, Faculty of Engineering, Chulalongkorn University, Bangkok 10330, Thailand
[d] National Nanotechnology Center (NANOTEC), National Science and Technology Development Agency (NSTDA), Pathum Thani 12120, Thailand
[e] Center of Excellence on Catalysis and Catalytic Reaction Engineering, Department of Chemical Engineering, Faculty of Engineering, Chulalongkorn University, Bangkok 10330, Thailand
[f] Bio-Circular-Green-economy Technology & Engineering Center, BCGeTEC, Faculty of Engineering, Chulalongkorn University, Bangkok 10330, Thailand
[g] Department of Chemistry, Faculty of Science, King Mongkut's Institute of Technology Ladkrabang, Chalongkrung Road, Ladkrabang, Bangkok 10520, Thailand
[h] Department of Applied Chemistry, School of Engineering, Tohoku University, 6-6-07 Aoba, Aramaki, Aoba-ku, Sendai, 980-8579, Japan

[+]Y. Maneewong and P. Lakhani contributed equally to this work.
* To whom correspondence should be addressed.
Tel.: +66(0)2 889-2138 ext. 6101-3; Fax: +66(0)2 889-2138 ext. 6129
Email address: atthapon.sri@mahidol.edu (A. Srifa)

Entry	Caption	Page No.
1	General information of materials.	**S3**
2	Characterization's techniques information.	**S3-S4**
Table S1	Summary of the XPS results obtained from the reduced catalysts.	**S5**
Table S2	Experimental data for kinetic constant.	**S6**
Table S3	Experimental data for activation energy.	**S7**
Table S4	Catalytic performance comparison of Ni-based catalysts for levulinic acid (LA) hydrogenation to γ-valerolactone (GVL), highlighting LA conversion and GVL yield.	**S8**
Table S5	ICP-OES analysis of fresh and spent catalysts.	**S9**
Figure S1	X-ray photoelectron spectroscopy (XPS) spectra of reduced and passivated catalysts: (a) and (b) Ni 2*p* and (c) Re 4*f* regions.	**S10**
Figure S2	Reusability of the NiRe-PS catalyst over five consecutive catalytic cycles under identical reaction conditions (160 °C, 10 bar H_2, 2 h, 0.1 g catalyst).	**S11**
Figure S3	^{1}H NMR spectrum of the reaction product obtained over the NiRe-PS catalyst.	**S12**
Figure S4	Spent catalyst characterization of NiRe-PS after the first catalytic run (a) TEM and elemental mapping; (b) XPS spectra of Ni 2*p* and Re 4*f* regions; (c) XRD patterns; and (d) TGA profiles.	**S13**

1 General information of materials.

MCM-41 was obtained from ACS Material LLC with a purity of 99%. Nickel(II) nitrate hexahydrate ($Ni(NO_3)_2·6H_2O$, CARLO ERBA, purity ≥ 98.5%) and ammonium perrhenate (NH_4ReO_4, Sigma-Aldrich Pte. Ltd., purity ≥ 99%) were used as the respective metal precursors for Ni and Re. A 25 wt.% ammonia solution was procured from ANaPURE™ (New Zealand). Levulinic acid (Sigma-Aldrich Pte. Ltd., 98% purity) and 2-propanol (QREC Chemical, analytical reagent grade, >99%) were used as the reactant and solvent, respectively. 2-PrOD (isotopic purity = 98 atom% D) and D_2 (isotopic purity = 99.8 atom% D) were purchased from Sigma-Aldrich Pte. Ltd. Deionized water was used throughout all synthesis and washing procedures. All chemicals were of analytical grade and used as received.

2 Catalyst Characterizations information.

The textural properties of the calcined catalysts were analyzed by N_2 physisorption at −196 °C using a BELSORP mini II (MicrotracBEL, Japan) gas sorption analyzer. The specific surface area was calculated by the BET method, while pore volume and pore size distribution were obtained from the desorption branch using the BJH model. The actual metallic contents of the calcined samples were determined by inductively coupled plasma-optical emission spectroscopy (ICP-OES, PerkinElmer NexION® 2000). Prior to analysis, solid samples were digested in acid under microwave irradiation. Chemisorption analyses were performed using a Quantachrome TPRWin v4.10 analyzer. H_2 temperature-programmed reduction (H_2-TPR) and temperature-programmed desorption of NH_3 and H_2 (NH_3-TPD and H_2-TPD) were conducted following established procedures to determine the reducibility, hydrogen uptake, and surface acidity of the catalysts. Raman spectroscopy (PerkinElmer Spectrum™ GX) was used to investigate the metal-support interactions and structural evolution of the calcined catalysts. The nature and strength of Lewis and Brønsted acid sites were examined using pyridine-adsorbed diffuse reflectance infrared Fourier-transform spectroscopy (pyridine-DRIFTS) on a Nicolet iS50 FTIR spectrometer equipped with a mercury–cadmium telluride (MCT) detector and a Harrick reaction cell (ZnSe windows). Samples were pretreated at 150 °C under Ar (30 sccm) for 1 h to remove physisorbed water, followed by in situ reduction in H_2 (30 sccm) at 450 °C for 3 h. After cooling to 30 °C, pyridine was adsorbed and spectra were recorded between 650-4000 cm^{-1} (4 cm^{-1} resolution, 64 scans). CO-DRIFTS was carried out using the same setup to probe surface metal sites. After activation, CO adsorption was performed at 0 °C using 10% CO/He (30 sccm for 20 min), and temperature-resolved spectra were recorded at 50, 100, 150, and 200 °C under flowing Ar. Additionally, time-resolved DRIFTS was employed to monitor LA adsorption and hydrogenation on activated catalysts at 140 °C under 10 bar H_2 for 0–40 min. The crystal structure of the calcined and reduced samples was examined using X-ray diffraction (XRD) over the 2θ range of 10°–80° (step time: 0.5 s). Structural evolution during in situ H_2 reduction (50–500 °C, held at 500 °C for 3 h) was investigated by in situ X-ray absorption spectroscopy (XAS) at Beamline 2.2, Synchrotron Light Research Institute (Thailand). The calcined samples were diluted with boron nitride (BN), pelletized, and analyzed in transmission mode at the Ni K-edge and Re L_3-edge using corresponding metal foils for energy calibration. Data were analyzed using the ATHENA software, while linear combination fitting (LCF) was used to quantify metallic fractions. Wavelet transform (WT) analyses were performed using the HAMA program (k-range: 0–15 $Å^{-2}$, R-range: 0–6 Å) with a Morlet wavelet. X-ray photoelectron spectroscopy (XPS) was performed using an AXIS SUPRA spectrometer (Kratos Analytical) with a monochromatic Al Kα X-ray source. The calcined samples were reduced ex situ at 500 °C for 3 h and passivated in 1% O_2/Ar for 1 h prior to measurement. Binding energies were calibrated to the C 1s peak at 284.6 eV, and spectra were deconvoluted using XPSPEAK41 software. The morphology, particle size distribution, and lattice fringes of the reduced catalysts were analyzed by transmission electron microscopy (TEM) and energy-dispersive X-ray spectroscopy (EDS) on a JEOL JEM-3100F microscope operated at 300 kV. Thermal stability and coke deposition of the reduced and spent catalysts were evaluated by thermogravimetric analysis (TGA, Mettler Toledo, Switzerland). The liquid products after catalytic reactions were separated using chloroform and analyzed by gas chromatography–mass spectrometry (GC-MS, Agilent 7890A) to identify reaction intermediates and products. Isotopic distribution in products obtained under H_2/D_2 or 2-propanol (2-PrOH) and deuterated analogue (2-PrOD) conditions was analyzed to elucidate hydrogen/proton participation during hydrogenation. ^{1}H NMR spectra were recorded on a Bruker Avance Ascend 600 MHz spectrometer using Topspin 4.4.1 software, employing D_2O for water-based and CD_3OD for 2-propanol-based reactions, confirming solvent-derived hydrogen transfer in the reaction mechanism.

Table S1 Summary of the XPS results obtained from the reduced catalysts.

Sample	Binding energy (eV)									Atomic concentration (%) [a]					Metallic Fraction	
	Ni 2p					Re 4f				Ni	Re	Si	C	O	Ni [b] (0)	Re [c] (0)
	Ni^0	NiO	Ni^{2+}	$Ni^{\delta+}$	Sat.	Re	Re^{4+}	Re^{6+}	Re^{7+}							
Ni-IM	852.3	854.0	855.5	856.5	860.5	-	-	-	-	1.2	0.0	30.7	6.0	62.1	0.24	-
NiRe-IM	852.9	854.0	855.7	856.7	860.4	40.7 42.75	41.4 43.78	45.4 48.4	46.8 49.2	1.1	0.2	30.3	5.8	62.6	0.11	0.08
Ni-PS	852.8	854.5	855.9	857.3	861.4	-	-	-	-	4.7	0.0	26.6	5.8	63.0	0.05	-
NiRe-PS	852.3	854.5	855.9	857.4	861.5	40.63 42.86	41.5 44	45.32 48.24	46.54 49.5	4.3	0.5	27.1	5.5	62.8	0.09	0.17

[a] atomic concentration calculated from XPS survey
[b] Ni (0) fraction calculated from the ratio of Ni (0) / (Ni (0) + Ni (2+))
[c] Re (0) fraction calculated from the ratio of Re (0) / (Re (0) + Re (4+) + Re (6+) + Re (7+))

Table S2 Experimental data for kinetic constant.

Reaction time (min) t	Experiment 1	Experiment 2	Experiment Average	SD	R^2
	$-\ln(1-X_{LA})$				
Ni-PS catalyst					
60	0.085416	0.110933	0.098174	0.018043	0.9837
90	0.135997	0.11877	0.127384	0.012181	
120	0.153979	0.133655	0.143817	0.014371	
150	0.151128	0.181795	0.166461	0.021685	
NiRe-PS catalyst					
60	0.303000	0.295427	0.299214	0.005355	0.9942
90	0.500939	0.494181	0.49756	0.004779	
120	0.712451	0.642765	0.677608	0.049275	
150	0.952098	0.957504	0.954801	0.003823	

Table S3 Experimental data for activation energy.

1/T (K)	Experiment $\ln r_{GVL}$ (mmol GVL g_{cat}^{-1} min^{-1})			SD	R^2
	1	2	Average		
Ni-PS catalyst					
0.0025	-10.0362	-9.96384	-10.0000	0.051166	0.9960
0.0024	-9.04133	-9.03213	-9.0367	0.006505	
0.0023	-8.28326	-8.3512	-8.3172	0.048041	
0.0022	-7.50786	-7.57072	-7.5393	0.044449	
NiRe-PS catalyst					
0.0027	-9.82799	-9.49612	-9.6621	0.234668	0.9556
0.0025	-8.64478	-8.6858	-8.6653	0.029006	
0.0024	-7.27682	-7.21071	-7.2438	0.046747	
0.0023	-6.66951	-6.67112	-6.6703	0.001138	

Table S4 Catalytic performance comparison of Ni-based catalysts for levulinic acid (LA) hydrogenation to γ-valerolactone (GVL), highlighting LA conversion and GVL yield.

Entry	Catalyst	Metal content (wt%)	solvent	T (°C)	time (h)	LA conv. (%)	GVL yield (%)	TOF (h^{-1})	Rate (mmol GVL/ g_{cat}^{-1} h^{-1})	Ref.
1	Ni3-Zn1@OMC	Ni:13.5 ,Zn: 5	Water	140	2	74	61	2.7	8.4	(Tang et al. 2023)[1]
2	Ni/Ru@WOMC	Ni: 9.6,Ru: 0.9	2-propanol	160	2	100	100	5.0	8.6	(Wang et al. 2023)[2]
3	30%Ni/O-clay450N	Ni: 26.31	1,4-Dioxane	140	5	100	100	1.3	5.7	(Kamble et al. 2023)[3]
4	Ni-Al	Ni: 53.30	Ethanol	140	2	100	97	4.5	41.2	(Shao et al. 2022)[4]
5	S3M1.5@NiPS-600	Ni: 24.3	Ethyl acetate, dodecane (internal standard)	150	3	95	91	1.9	7.9	(Li, Hsieh, and Lin 2022)[5]
6	1-Ni/C-400	Ni: 6.6	water	160	3	100	95	7.2	8.1	(Fang et al. 2019)[6]
7	500-NiFe NPs@C (3:1)	Ni: 14.95, Fe: 4.93	isopropanol	130	2	94	90	2.2	7.5	(Wang et al. 2018)[7]
8	Ni@FLG-600	Ni : 57.5	water (1,4-dioxane:internal standard)	130	7	99	99	0.2	1.8	(Zhang, Li et al. 2025)[8]
9	$NiRe_{0.075}/Al_2O_3$	Ni: 10.1 ,Re: 2.5	2-propanol	160	2	100	93	10.8	20.1	(Y. Maneewong et al. 2025) [9]
10	NiRe-PS	Ni : 8.1, Re :2.3	2-propanol	160	2	100	91.6	26.3	39.4	This work

Table S5 ICP–OES analysis of fresh and spent catalysts.

Sample	Elemental Composition from ICP (%)	
	Ni (wt%)	Re (wt%)
Fresh NiRe-MCM41-PS	8.1	2.3
NiRe- PS After 1st run	6.9	2.3
NiRe- PS After 5th run	6.8	1.9

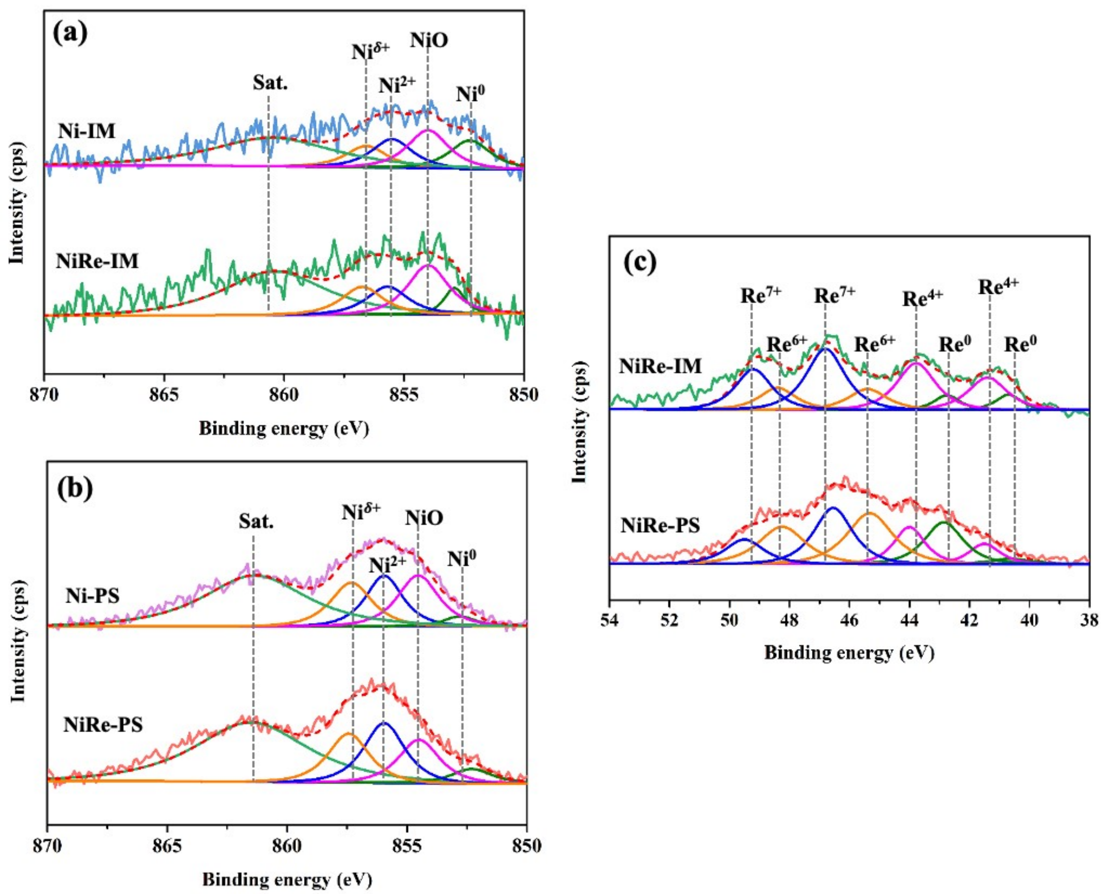

Figure S1 X-ray photoelectron spectroscopy (XPS) spectra of reduced and passivated catalysts: **(a)** and **(b)** Ni 2*p* and **(c)** Re 4*f* regions.

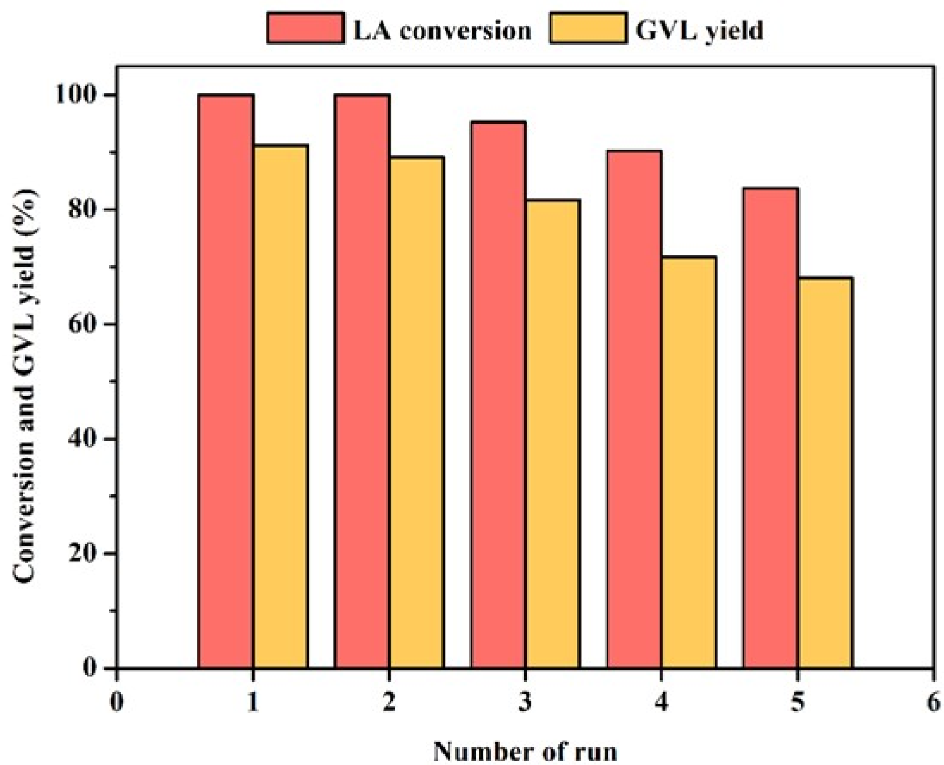

Figure S2 Reusability of the NiRe-PS catalyst over five consecutive catalytic cycles under identical reaction conditions (160 °C, 10 bar H_2, 2 h, 0.1 g catalyst).

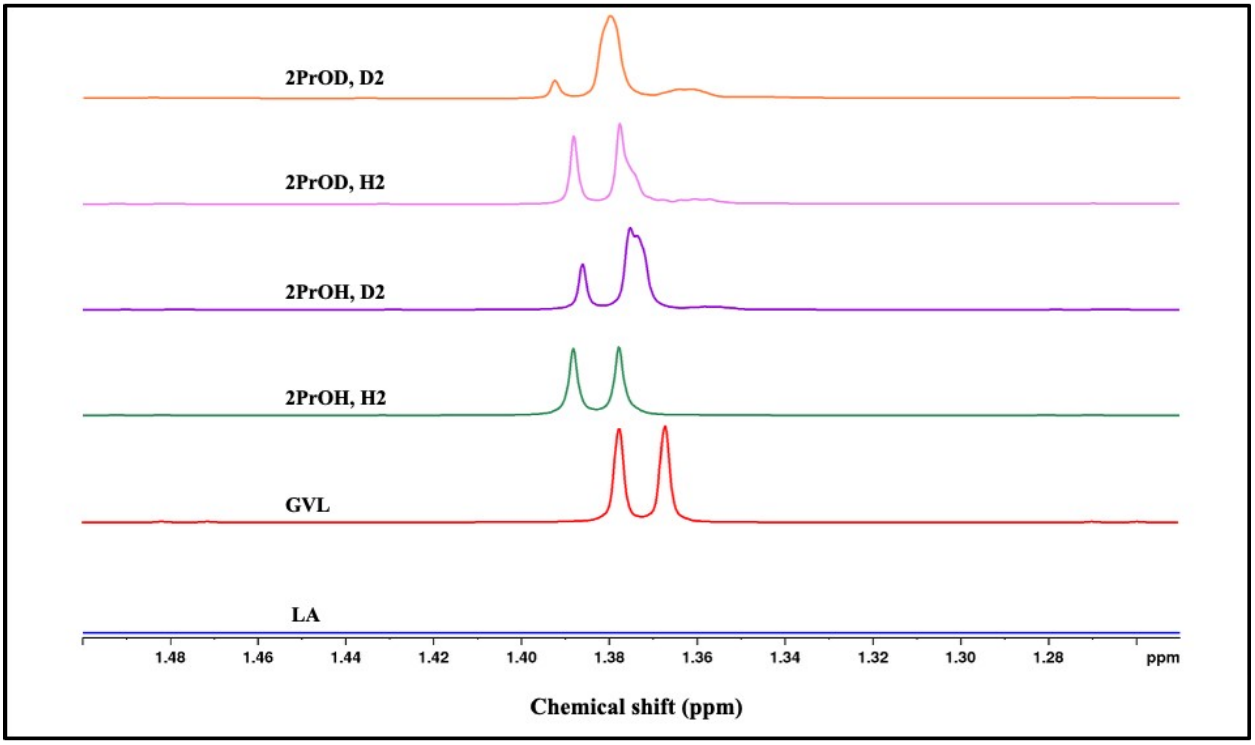

Figure S3 ^{1}H NMR spectrum of the reaction product obtained over the NiRe-PS catalyst.

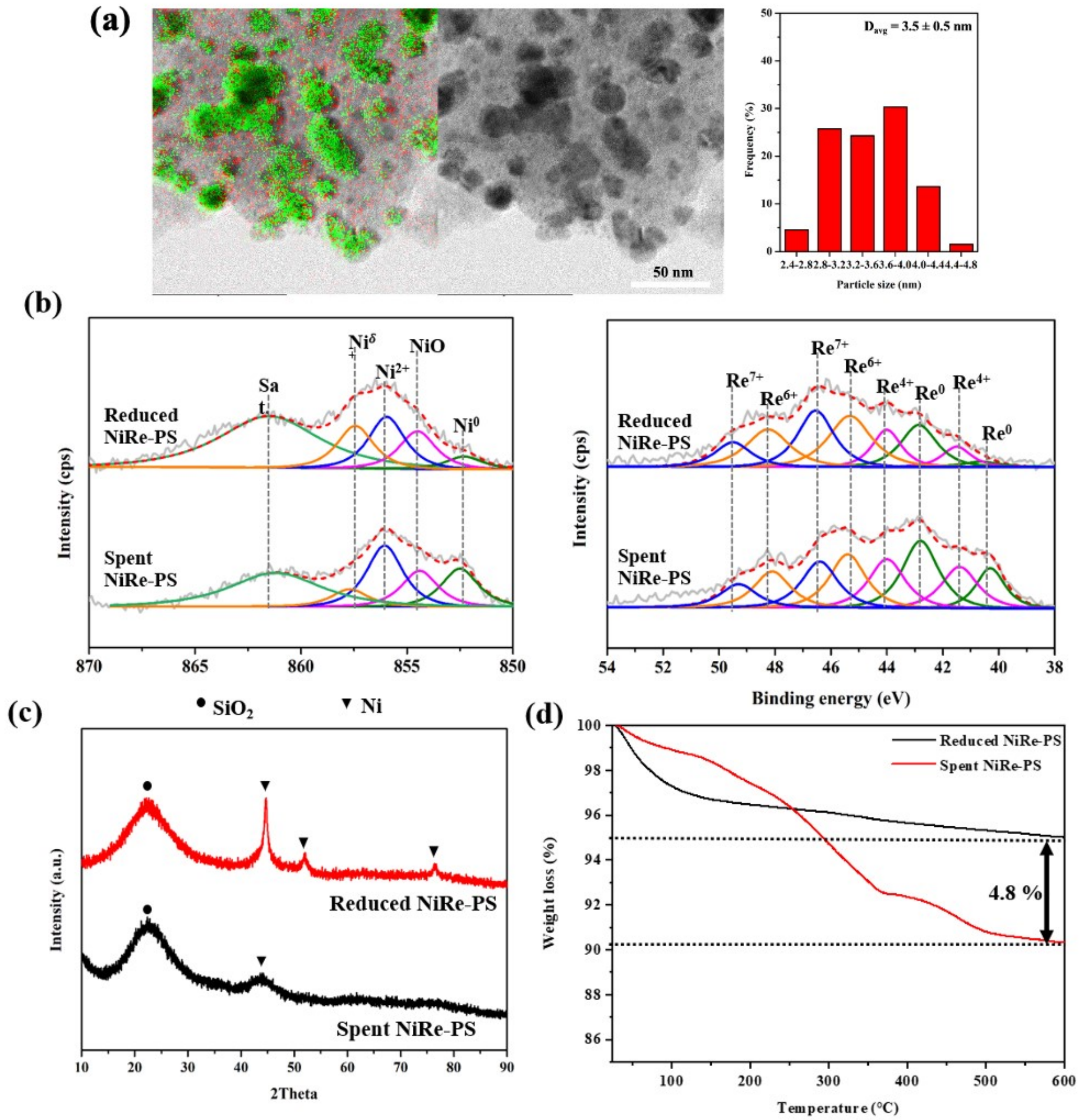

Figure S4 Spent catalyst characterization of NiRe-PS after the first catalytic run (160 °C, 2 h, 0.1 g catalyst, 10 bar H_2): (a) TEM and elemental mapping showing uniform Ni (green) and Re (red) dispersion with minimal agglomeration; (b) XPS spectra of Ni 2*p* and Re 4*f* regions revealing slight surface oxidation of Ni^0 and Re^0 after reaction; (c) XRD patterns confirming preserved mesostructure with minor Ni peak attenuation; and (d) TGA profiles showing increased weight loss due to minor carbonaceous deposition.

References

1. Y. Tang, J. Fu, Y. Wang, H. Guo and X. Qi, *Fuel Processing Technology*, 2023, **240**, 107559.
2. X. Wang, X. Qi, M. Qiu, F. Shen, J. Yang and B. Shen, *Fuel*, 2023, **341**, 127720.
3. P. A. Kamble, C. Vinod, V. K. Rathod and M. L. Kantam, *Catalysis Today*, 2023, **408**, 36-49.
4. Y. Shao, K. Sun, M. Fan, J. Wang, G. Gao, L. Zhang, S. Zhang and X. Hu, *Chemical Engineering Science*, 2022, **248**, 117258.
5. C.-C. Li, C.-H. Hsieh and Y.-C. Lin, *Molecular Catalysis*, 2022, **523**, 111720.
6. S. Fang, Z. Cui, Y. Zhu, C. Wang, J. Bai, X. Zhang, Y. Xu, Q. Liu, L. Chen and Q. Zhang, *Journal of Energy Chemistry*, 2019, **37**, 204-214.
7. H. Wang, C. Chen, H. Zhang, G. Wang and H. Zhao, *Chinese Journal of Catalysis*, 2018, **39**, 1599-1607.
8. Y. Zhang, Y. Li, C. Shen, C. Yang, H. Wu, C. Jiang, S. Chen, M. Li, Y. Li and W. Ding, *Applied Catalysis B: Environment and Energy*, 2025, **361**, 124595.
9. Y. Maneewong, P. Nimmanterdwong, S. Ratchahat, C. Sakdaronnarong, W. Limphirat, P. Khemthong, B. Rungtaweevoranit, K. Faungnawakij, S. Assabumrungrat and Y.-C. Lin, *Chemical Engineering Journal*, 2025, **508**, 160969.